Manuscript TOXSCI-17-0705

Manuscript:

Proteomic comparison of various hepatic cell cultures for preclinical safety pharmacology

Authors and affiliations:

Tracey Hurrell* (tracey.hurrell@ki.se)

Charis-Patricia Segeritz† (charis.walko@gmail.com)

Ludovic Vallier† (lv225@cam.ac.uk)

Kathryn S. Lilley‡ (k.s.lilley@bioc.cam.ac.uk)

Allan Duncan Cromarty* (duncan.cromarty@up.ac.za)

* Department of Pharmacology, Faculty of Health Sciences,
School of Medicine, University of Pretoria, South Africa

† Wellcome Trust–Medical Research Council Stem Cell Institute,
Anne McLaren Laboratory for Regenerative Medicine, Department of Surgery,
University of Cambridge, Cambridge, CB2 0SZ, United Kingdom

‡ Cambridge Centre for Proteomics, Department of Biochemistry,
University of Cambridge, Tennis Court Road, Cambridge CB2 1QR, United Kingdom

Correspondence:

Tracey Hurrell
Department of Pharmacology
Faculty of Health Sciences
University of Pretoria
Private Bag X323
Pretoria
0007
tracey.hurrell@ki.se

Financial support:

National Research Foundation Thuthuka Funding Scheme (Grant No. 87880.)

UK Commonwealth Split-site Scholarship (ZACS-2014-653)

Commonwealth, European and International Cambridge Trust Scholarship

Abstract

Experimental drugs need to be screened for safety within time constraints. Hepatotoxicity is one concerning contributor to the failure of investigational new drugs and a major rationale for postmarketing withdrawal decisions. Ethical considerations in preclinical research force the requirement for highly predictive *in vitro* assays using human tissue which retains functionality reflective of primary tissue. Here, the proteome of cells commonly used to assess preclinical hepatotoxicity was compared. Primary human hepatocytes (PHHs), hepatocyte-like cells differentiated from human pluripotent stem cells (HLCs), HepG2 cell monolayers and HepG2 cell three dimensional (3D) spheroids were cultured and collected as whole cell lysates. Over 6000 proteins were identified and quantified in terms of relative abundance in replicate proteomic experiments using isobaric tagging methods. Comparison of these quantitative data provides biological insight into the feasibility of using HLCs, HepG2 monolayers and HepG2 3D spheroids for hepatotoxicity testing. Collectively these data reveal how HLCs differentiated for 35 days and HepG2 cells proteomes differ from one another and that of PHHs. HepG2 cells possess a strong cancer signature and do not express adequate abundance of key metabolic proteins which mark the hepatic phenotype, this was not substantially altered by culturing as 3D spheroids. These data suggest that while no single hepatic model reflects the diverse array of outcomes required to mimic the *in vivo* liver functions that HLCs are the most suitable investigational avenue for replacing PHHs *in vitro*.

Keywords

Hepatotoxicity, labelled proteomics, systems biology, hepatocyte-like cells, HepG2 cells, spheroids

Introduction

Disappointing drug approval rates suggest that the pharmaceutical golden era is over. Unprecedented challenges facing the pharmaceutical industry include high preclinical and clinical termination and attrition rates, patent expirations as well as regulatory and other governing policies (Cai J *et al.*, 2012; DiMasi JA *et al.*, 2003). Safety Pharmacology Studies for Human Pharmaceuticals (ICH-S7A and ICH-S7B) govern policies for the identification of undesirable pharmacodynamic effects on the "core battery" of vital organ systems: central nervous, respiratory and cardiovascular (Redfern WS *et al.*, 2002). Studies of other organ systems are often based on the nature of the candidate drug which then less rigorously assesses organ toxicities such the liver. The number of drugs resulting in drug-induced liver injury (DILI) are a noteworthy burden for the pharmaceutical industry as there are no universal approaches for early identification of hepatotoxic potential prior to R&D commitment (Ballet F, 1997). *In vitro* models for assessing drug metabolism and safety need to be sufficiently sensitive and reproducible to extrapolate to *in vivo* counterparts. Beyond the cellular diversity of the liver, the biophysical and biochemical properties of extracellular matrices influence cellular behaviour (LeCluyse EL *et al.*, 2012). Successful prediction of *in vitro* hepatotoxicity relies on the state of hepatocyte differentiation, degree of cellular functionality, exposure duration and type of investigational drug (Knasmüller S *et al.*, 2004; Xu JJ *et al.*, 2004). Freshly isolated primary human hepatocytes (PHHs) remain the "*gold standard*". PHHs are lifespan restricted and unable to proliferate *ex vivo* but express all major metabolising enzymes and transporter proteins. Decreased cytochrome-related functions and liver-specific gene expression have historically been of concern (LeCluyse EL *et al.*, 2012; Mills JB *et al.*, 2004) but can be circumvented or minimized under the appropriate culture conditions (Bell CC *et al.*, 2016; Vorrink SU *et al.*, 2017). Other hepatocyte sources include immortalized cell lines and hepatocytes derived from human induced pluripotent stem cells (hiPSCs) which possess bipotent differentiation potential. Immortalized cell lines, such as HepG2 cells, are still commonly used as surrogated for hepatocytes *in vitro* (Mingard C *et al.*, 2018; Paech F *et al.*, 2018; Ramirez T *et al.*, 2018; Shah U-K *et al.*, 2018) despite being associated with unreliable expression of bio-transforming enzymes and discontinuous phenotype and function (Duret C *et al.*, 2007; LeCluyse EL *et al.*, 2012). Adhesive cues, growth factors, intercellular contact, mechanical forces, cell shape and extracellular matrix, geometry and spatial organisation and other environmental mechanics are reported to dictate cellular functionality (Bhadriraju K *et al.*, 2002). Monolayer cell cultures oversimplify the complexity of organ systems which misrepresent the original phenotype (Bhadriraju K *et al.*, 2002; Peters TS, 2005). Cellular dependence on "*community behaviour*" has put an emphasis on three dimensional (3D) cultures which spatially organise and better resemble the *in vivo* cellular architecture (Fey SJ *et al.*, 2012).

To determine which cell model approximates the proteome of PHHs with the greatest fidelity, thereby implying a relevant pharmaceutical screening platform, we compared the proteome of pooled donor primary human hepatocytes with differentiated hepatocyte-like cells (HLCs) as well as monolayer and 3D spheroid cultured human hepatocyte-derived cell lines using stabled isotope labelled mass spectrometry. Our results suggest that approximating the proteome of PHHs was limited in all cell models investigated but that HLCs are a more suitable replacement for PHHs under the conditions in this study.

Materials and methods

Pooled primary human hepatocytes

Cryopreserved pooled primary human hepatocytes (10 donors; Lot number HUE50D, Gibco Lifeline Cell Technology) were purchased. Hepatocytes were thawed in pre-warmed Hepatocyte Recovery Medium (Gibco Lifeline Cell Technology). Cells were resuspended in plating medium (Williams E Medium containing 5% foetal bovine serum (FBS), 1 µM dexamethasone, 1% penicillin-streptomycin, 4 µg/ml human recombinant insulin, 2 mM GlutaMAX™ and 15 mM HEPES; pH 7.4). PHHs were culture in suspension at $2x10^6$ cells/well for 4 hours at 37°C to remove cellular debris and minimise the effects of dedifferentiation on the proteome.

HepG2 cell monolayers and 3D spheroids

Human hepatoma cells (85011430-1VL) were obtained from the European Collection of Cell Cultures (ECACC; Wiltshire, United Kingdom). HepG2 cells were cultured in EMEM supplemented with 10% FBS, 1% penicillin-streptomycin and 2 mM L-glutamine and incubated at 37°C with 5% CO_2. For HepG2 3D spheroids, cells were seeded Perfecta3D® 96-well hanging drop plates (3D Biomatrix; Michigan, USA) at 10 000 cells/well in 45 µl medium. Cells aggregated under gravity with partial exchange of growth medium every alternate day. Cells were seeded from the same stock and then harvested appropriately for each culture format. HepG2 monolayers were seeded at a moderate to high density and harvested once confluence was reached at day 3. Seeding density of HepG2 3D spheroids for obtain a high protein yield was titrated to viability and were therefore cultured for 10 days.

Hepatocyte-like cell differentiation

Human induced pluripotent stem cells (hiPSCs) were generated as previously reported (Hannan NR *et al.*, 2013; Rashid ST *et al.*, 2010; Yusa K *et al.*, 2011). An α1-anti-trypsin deficient hiPSC line was wild-type corrected (Glu342Lys; SERPINA 1) using a targeted biallelic gene correction of the homozygous Z mutation. Corrected hiPSCs had 29 mutations in protein-coding exons, 22 were which

were splice site mutations or non-synonymous and not found to alter differentiation (Yusa K *et al.*, 2011). Stable hiPSCs colonies, from a single clone, were cultured in chemically-defined medium with polyvinyl alcohol (CDM-PVA: 250 ml Iscove's Modified Dulbecco's Media, 250 ml Ham's F12 + GlutaMAX, 1% concentrated lipids, 0.7% insulin, 0.14% transferrin, 0.1% PVA, 1% penicillin/streptomycin) supplemented with Activin A (10 ng/ml) and FGF-2 (12 ng/ml) in a tri-gas incubator (5% O_2, 5% CO_2, 90% N_2), maintained at 37°C. Differentiation (Figure 1) was conducted as previously reported (Hannan NR *et al.*, 2013) and samples were collected after 35 days where a peak in functional activity was observed (data not shown).

Sample collection, protein quantitation and SDS-PAGE

Cells were lysed, on ice, using a buffer containing 10 mM Tris-HCL, 1 mM EDTA, 0.5 mM EGTA, 1% Triton X-100, 0.1% SDS, 0.1% sodium deoxycholate, 140 mM sodium chloride and cOmplete™ protease inhibitor cocktail (Roche Pharmaceuticals; Basel, Switzerland). Cellular disruption was performed using an ultrasonic bath (120W) for 5 minutes with 30 second pulses. Supernatant protein was quantified using the bicinchoninic acid assay with a 1:50 ratio of Reagent B (4% copper II sulfate pentahydrate) to Reagent A (2% sodium carbonate, 0.16% sodium tartrate, 0.9% sodium bicarbonate and 1% BCA; pH 11.25). Protein (20 µg) was mixed 1:1 with Laemmli sample buffer (0.125 M Tris-HCL (pH 6.8), 4% SDS, 20% glycerol, 5% β-mercaptoethanol, 0.004% bromophenol blue) and loaded onto precast Mini-PROTEAN TGX polyacrylamide gels (4-15%). Proteins were separated using a Mini-PROTEAN Tetra System at 80 V (15 minutes) to 160 V. Gels were stained using 0.1% Coomassie brilliant blue and scanned using a Bio-Rad Gel-Doc EZ Imager.

Protein digestion and isobaric tagging

Replicates of each sample (n=6 for HLCs, n=4 for PHHs, n=4 for HepG2 monolayers, n=3 for HepG2 3D spheroids) were labelled with different 6-plex tandem mass tags (TMT; Thermo Fischer Scientific Inc.; Maryland, USA). Fifty micrograms of protein was reduced with 10 mM dithiothreitol at 37°C and then alkylated with 25 mM iodoacetamide for 2 hours at room temperature. Proteins were precipitated overnight with 100% acetone at 4°C, harvested by centrifugation at 16 000 *g* and resuspended in 100 mM HEPES (pH 8.5). Samples were digested with 1.25 µg (1:40) sequence-grade modified trypsin for 1 hour at 37°C. Additional trypsin (1:40) was added and digestion continued overnight at 37°C. Tags were resuspended in 41 µl mass spectrometry-grade acetonitrile. Digested peptides were clarified for 20 minutes at 16 000 *g* and the supernatant labelled for 2 hours at room temperature under constant agitation. Labelling was quenched with 8 µl of 5% hydroxylamine for 1 hour and further quenched overnight at 4°C with dH_2O. Labelled samples were combined to contain all 6-plex labelled samples and reduced to dryness.

Solid phase extraction and peptide fractionation

Labelled peptides were solubilized in dH_2O with 0.1% trifluoroacetic acid (TFA) and loaded onto a conditioned SepPak C18 cartridge (100 mg). Desalting was conducted by washing with 0.1% TFA and 0.5% acetic acid and peptides were eluted in 70% acetonitrile with 0.05% acetic acid. Eluents were vacuum dried and resuspended in 100 µl of 20 mM ammonium formate (pH 10) with 4% acetonitrile. Sample complexity was reduced by peptide fractionation using a Waters ACQUITY system. Peptides were loaded via a single partial loop injection, onto a Waters ACQUITY UPLC BEH C18 column (130Å, 2.1 x 150 mm, 1.7 µm). Peptides were profiled at 0.25 ml/minute using an initial isocratic low organic phase (mobile phase A: 20 mM ammonium formate; pH 10 and mobile phase B: 80% acetonitrile, 20 mM ammonium formate; pH 10) followed by a 50 minute linear gradient of increasing percentage (5-60%) mobile phase B. Chromatography was monitored using a diode array detector scanning between 200-400 nm. Fractions with eluted peptides were dried and pooled into 15 samples using 0.1% formic acid for liquid chromatography tandem-mass spectrometry (LC-MS/MS) analysis.

Mass spectrometry

Samples were analysed using a Dionex Ultimate 3000 RSLCnano LC system and a Thermo Scientific Q Exactive Hybrid Quadrupole-Orbitrap Mass Spectrometer. Peptides (1-2 µg) were loaded onto an Acclaim PepMap 100 C18 pre-column (100Å, 300 µm x 5 mm, 5 µm) using an Ultimate 3000 auto-sampler with 0.1% formic acid for 3 minutes at a flow rate of 10 µl/minute. Switching the column valve eluted peptides onto a PepMap C18, EASY-Spray LC analytical column (100Å, 75 µm x 500 mm, 2 µm). Peptide separation was profiled at 300 nl/minute by applying a 100 minute linear gradient of 4-40% using mobile phase A (H_2O with 0.1% formic acid) and mobile phase B (80% acetonitrile, 20% H_2O with 0.1% formic acid) over a 120 minute total run time. Mass spectrometry measured the mass-to-charge ratios (m/z) in positive ion data-dependent mode. Full MS scans were performed in the range of 380-1500 m/z at a mass resolution of 70 000 with an automatic gain control (AGC) of $5x10^6$ at a maximum injection time of 250 ms. Data dependent scans of the top 20 most abundant ions, with charge states between 2+ and 5+, were automatically isolated, selected and fragmented by higher energy collisional dissociation (HCD) in the quadrupole mass analyser. Dynamic exclusion was set at 60 seconds. HCD fragmentation was performed at a normalized collision energy (NCE) of 32.5% and a stepped NCE of 10% and monitored at a resolution of 17 500. The AGC, maximum injection time, first fixed mass and isolation window for MS2 scans was $5x\ 10^4$, 150 ms, 100 m/z and 1.2m/z respectively.

Data processing

Raw files were converted using ProteoWizard MSConvertGUI (Kessner D *et al.*, 2008) with peak picking and a threshold count of 150 used as conversion filters. Peak lists were searched against a UniProtKB/Swiss-Prot human database (Homo sapiens, Canonical sequences, January 2016, Sequences: 20 194) using SearchGUI version 2.3.1 (Vaudel M *et al.*, 2011) with X!Tandem, MS-GF+ and Comet search engines. Post-processing of peptide-spectrum matches (PSM) for protein identification was done using Peptide Shaker version 1.7.3 (Vaudel M *et al.*, 2015). Search parameters included: minimum and maximum precursor mass of 300 and 900 Da respectively, precursor mass tolerance of 10 ppm, fragment mass tolerance of 0.2 Da and a maximum number of 2 missed cleavages. Fixed modifications were set to include S-carbamidomethyl cysteine, TMT 6-plex modification of lysine and peptide N-termini with variable modifications including oxidation of methionine and deamidation of asparagine or glutamine. Reporter version 0.2.13 (http://compomics.github.io/projects/reporter.html) was used for relative quantification of TMT reporter ions. Deisotoping using label specific purity coefficients and relative quantification was conducted in Reporter version 0.2.13 (http://compomics.github.io/projects/reporter.html).

Data analysis and visualisation

Proteins present in replicates, identified with 2 unique peptides and 100% confidence, were analysed in Perseus version 1.5.3.1 (Max Planck Institute of Biochemistry). Average protein ratios, with the associated standard deviation, were produced and generic protein clusters identified using Euclidean distances from reference profiles. K-mean pre-processing and average linkages were used for hierarchical clustering. Multi-sample testing was conducted, on log2(x) transformed relative abundance ratios, using ANOVA with a permutation-based false discovery rate (FDR) for truncation at an FDR of 0.01 with results reported as q-values. Volcano plots were generated using two-tailed t-tests and stringency of analysis controlled with an FDR of 0.01 with 250 randomizations, mean weighting and the difference and -Log(P-value) were used to assign significance (q-value). In addition, proteins were annotated for gene ontology (GO) biological processes (BP), molecular functions (MF), cellular components (CC) as well as Reactome and KEGG pathway identifiers.

Results

This study includes proteomic comparisons which, to date, are absent from literature. Here, PHHs were compared to hiPSC-derived HLC monolayers, HepG2 monolayers and HepG2 3D spheroids (Figure 2A-C) using replicates of quantitative proteomics. Protein-mass profiles of the various hepatocyte lysates clearly demonstrated proteomic differences (Figure 2D). The stabled isotope

labelled proteomics workflow applied to these lysates identified and quantified 6682, 6285 and 6449 proteins for replicates 1 to 3 respectively. Filtering proteins for those identified by at least 2 unique peptides at 100% identification confidence reduced the cohort to 5231 proteins across triplicate TMT experiments.

Hierarchical clustering of PHHs, HLCs, HepG2 monolayers and HepG2 3D spheroids

Hierarchical clustering, of the 5231 proteins, predominantly grouped samples according to cell type with distinctive grouping of PHHs, HLCs and HepG2 monolayers and HepG2 3D spheroids (Figure 3A). PHHs and HLCs co-segregated separately from HepG2 cells with the exception of PHH3 which clustered with HepG2 3D spheroids. Identification of PHH3 as an outlier could be due to biological variance induced thawing, quantity of labelled protein or reduced labelling efficiency. Despite this behaviour of PHH3, hierarchical clustering of biological replicates which identified protein groupings with abundance trends unique to specific cell types (Figure 3B). Here, cluster 4 (254 proteins) were increased in HLCs, cluster 5 (44 proteins) increased in both HLCs and PHHs, cluster 6 (30 proteins) and cluster 8 (10 proteins) both increased in HLCs only (Supplementary data 2: Hierarchical clustering). In addition, generic clustering provided 100 groups of more tightly regulated trends to investigate more conservative protein relationships (Supplementary data: Generic clustering_100).

Principal component analysis of PHHs, HLCs, HepG2 monolayers and HepG2 3D spheroids

Principal component analysis (PCA) clustered PHHs, with the exception of PHH3, and HLCs distinctly in Component 1 (40.5%) and Component 2 (33.2%) of principal component space (Figure 4A). In contrast, HepG2 cells, regardless of culturing strategy, clustered together in these components. This suggests that when collapsing the data into new linear combinations that HepG2 monolayers and 3D spheroids are seemingly indistinguishable when compared to the proteome of either PHHs or HLCs. However, comparing Component 1 and Component 3 (4.8%) of the PCA (Figure 4B) spatially resolved HepG2 monolayers and HepG2 3D spheroids suggesting that differences based on culture technique do potentially alter the proteome but are confounded by the degree to which these cells differ from PHHs. Lower components, accounting for less overall variance (Component 4: 4.3% to Component 16: 0.6%) did not provide additional insight into clustering (data not shown).

Comparison of PHHs versus HLCs

Direct comparison, using significance and fold change, of the PHH proteome identified 961 proteins increased and 1020 decreased in abundance in HLCs (Figure 5A). These 1981 proteins which differ in abundance, with the corresponding difference and q-value were reported (Supplementary data 2:

Volcano plot_PHHvHLCs). Of these, many proteins with higher abundance in PHHs were involved in metabolism including aldoketo reductase family 1 member C2, CYP4V2, mitochondrial aldehyde dehydrogenase X, alcohol dehydrogenase 6, mitochondrial dimethylglycine dehydrogenase and, solute carrier family 22 member 7 responsible for organic anion transport. Abundant proteins in HLCs included Kunitz-type protease inhibitor 2 (-log p-value: 5.042 and difference: -3.104) an inhibitor of hepatocyte growth factor activator. Other abundant proteins were involved in cytoskeletal arrangement such as coactosin-like protein, microtubule-associated protein 1B responsible for tyrosination of alpha-tubulin, macrophage-capping protein and, serine/threonine-protein kinase PAK 1 with roles in cytoskeleton dynamics, cell adhesion, migration, proliferation, apoptosis and mitosis (TheUniProtConsortium, 2014).

Comparison of PHHs HepG2 monolayers

Compared to PHH protein abundance, 956 and 1327 proteins were increased and decreased in HepG2 monolayers respectively (Figure 5B). These 2283 proteins which differed in abundance (Supplementary data 2: Volcano plot_PHHvHepG2) accounted for approximately 40% of the quantified proteins making HepG2 monolayers the most divergent from PHHs in direct comparison. Many proteins with greater abundance in PHHs were mitochondrial in origin and essential to facilitate hepatic functions such as energy production and catalysis. These included mitochondrial cytochrome b-c1 complex subunit which generates electrochemical potential coupled to ATP synthesis, mitochondrial aminomethyltransferase which catalyses glycine degradation, glycogenin-2 which serves as substrate for glycogen synthase, nicotinamide N-methyltransferase involved in xenobiotic metabolism, and solute carrier organic anion transporter family member 1B1 (TheUniProtConsortium, 2014). The decreased abundance in mitochondrial proteins could also be associated with the transformed phenotype of cancer cell lines which alters overall metabolic, glycolytic and anaerobic activity.

Proteins with greater abundance in HepG2 monolayers than PHHs, included multiple ubiquitous actin-associated proteins. This could be as a result of the unnatural microenvironment produced in monolayer cultures where HepG2 cells display cell protrusions for motility and migration not seen *in vivo* or in suspensions of PHHs. Actin-associated proteins functioning as intracellular anchors, scaffolds and signalling proteins, included protein enabled homolog, microtubule-associated protein 1B, fascin which organizes filamentous actin into bundles and filamin-A required for orthogonal branching and linking of actin filaments to membrane glycoproteins (TheUniProtConsortium, 2014).

Comparison of PHHs versus HepG2 3D spheroids

Compared to PHH protein abundance, 180 proteins increased and 683 decreased in abundance in HepG2 3D spheroids (Figure 5C). These 862 proteins accounted for only 18.8% (180 versus 956) and 51.4% (682 versus 1327) of the variance seen in HepG2 monolayers (Supplementary data 2: Volcano plot_PHHvHepG2(3D)). Here approximately 2.5-fold less proteins meets statistical cut-offs compared to HepG2 monolayers. Abundant proteins in PHHs compared to HepG2 3D spheroids, again included many mitochondrial proteins including cytochrome b-c1 complex subunit, ATP synthase subunit and cytochrome c oxidase subunit 6C. ADME associated proteins were more abundant in PHHs and included dimethylaniline monooxygenase [N-oxide] 4 involved in oxidative metabolism of xenobiotics, retinol dehydrogenase 16, CYP2D6, alpha-1-antichymotrypsin, alpha-1-acid glycoprotein 1, sideroflexin-5 a transmembrane citrate transport and StAR-related lipid transfer protein 5 responsible for intracellular transport of sterols or other lipids (TheUniProtConsortium, 2014). These data suggest that despite less proteins which differ in abundance that the source of these differences may not be related to enhancing the hepatic phenotype.

Comparison of overall differences in protein expression

Multiple sample testing (ANOVA) reported 684 proteins of 5231 (13%) with non-significant q-values (Supplementary data 2: ANOVA, non-significant). These proteins were predominantly ribosomal, ER, mitochondrial, transcriptional or translational associated proteins. However, side-by-side comparison of PHHs compared to HLCs, HepG2 monolayers or HepG2 3D spheroids demonstrated 1981, 2283 and 862 proteins respectively which were altered in abundance. This posed a series of questions: Were the same proteins increased or decreased in abundance in HLCs, HepG2 monolayers and HepG2 3D spheroids? Were some proteins increased in one model yet decreased in another? Therefore, proteins above significance thresholds in volcano plots were compared to determine if protein differences were conserved between HLCs, HepG2 monolayers and HepG2 3D spheroids (Table 1). These comparisons (HLCs versus HepG2 monolayer, HLC versus HepG2 3D spheroid or HepG2 monolayer versus HepG2 3D spheroid) suggest that where abundance was lower compared to PHHs it was common to HLCs, HepG2 monolayers and 3D spheroids. However, when proteins were increased in abundance compared to PHHs it was specific to HLCs, HepG2 cell monolayers or HepG2 3D spheroids. Further comparisons identified 62 proteins that displayed contrary abundance between HLCs and HepG2 monolayers and only 11 proteins HepG2 3D spheroids. In total, for HLCs and HepG2 cells, only 73 proteins were differential in their comparison to PHHs which accounted for only 1.4% (73 of 5231) of the total proteins analysed (Supplementary data 2: Model comparison). Proteins with higher abundance in HepG2 cells compared to HLCs were

principally associated with DNA replication, transcription and translation. Cell proliferation does not occur in HLCs during maturation which is in contrast to HepG2 cells which propagate indefinitely. This notably high abundance in HepG2 cells suggests that continual replication is a key factor restricting the mimicry of terminally-differentiated PHHs and mature hiPSC-HLCs.

Comparison of liver enriched and metabolic proteins

Correlating abundance of proteins suggested throughout literature (Baxter M *et al.*, 2015; Lemaigre F, 2010; Schwartz R *et al.*, 2014; Si-Tayeb K *et al.*, 2010; Uhlén M *et al.*, 2015) to describe the liver enriched proteome (Supplementary 1: Table 1) and those integral to hepatic metabolic function was done (Table 2). Data was interrogated for Phase I and II metabolic enzymes, CYP450s, monoamine oxidases, flavin-containing oxygenases, esterases, UGTs, sulfotransferases, N-acetyl transferases, glutathione S-transferases and transmembrane transporters. Relationships were tabulated as ANOVA significant as well as t-test significant to highlight the difference across each model. All of the major CYP isoforms (CYP3A4/5, CYP2D6, CYP2C8/9, CYP1A2, CYP2C19 and CYP2B6) were identified in PHHs but other model were most limited in expression of these enzymes. HLCs and HepG2 cells mostly displayed difference in t-test significance across the extracted proteins cohorts. Differences in relative protein abundance of some alcohol and aldehyde dehydrogenases, UDP-glucuronosyltransferases, glutathione S-transferases and cytochromes (CYP2C8, CYP2B6, CYP2S1, CYP4F12) was observed in HepG2 3D spheroids compared to equivalent monolayer cultures .

Discussion

Human-derived hepatic cells remain central to the applicability and performance of innovative liver models (Sison-Young RL *et al.*, 2015). Generating extensive protein expression profiles are required to ascertain that each model systems is “fit-for-purpose”. Comparable reports have previously quantified an 2722 proteins in three human-derived hepatic cell lines (HepG2, Upcyte, and HepaRG) compared to cryopreserved PHHs. Hierarchical clustering also segregated PHHs from the other cell types with ADME proteins being an influential factor (Sison-Young RL *et al.*, 2015). The higher depth of protein coverage reported in our study provides additional insight into hepatic phenotypes.

PCA and hierarchical clustering on the full complement of quantified proteins demonstrated that the HLCs proteome are more closely correlated to PHHs. PHHs are non-transformed and maintain the highest differentiation in status while HepG2 express a strong cancer signature. Considering this, it is suggested that in PCA Component 1 appears capable of separating samples based on whether the cells are transformed (HepG2 cells) or non-transformed (PHH and HLC) whereas Component 2 is distinguishing the level of differentiation.

Glucocorticoids, such as dexamethasone, through interaction with glucocorticoid receptors modulate gene transcription and cellular function. As a major regulator of cellular function, the absence of glucocorticoids in the HepG2 cell medium, while present in HLCs differentiation medium could contribute to the PCA clustering. Psarra *et al.* suggested that dexamethasone induces mitochondrial transcription factors including transcription factors A, B1 and B2 as well as oxidative phosphorylation genes such as cytochrome b (Psarra A-MG *et al.*, 2011). Mitochondrial transcription factor A (Q00059) was non-significant for each t-test comparison whereas mitochondrial dimethyladenosine transferase 1 (Q8WVM0) and 2 (Q9H5Q4) differed in HepG2 monolayers and HLCs respectively. Furthermore, cytochrome b5 (P00167) differed in all comparisons to PHHs regardless of the presence or absence of glucocorticoids. This illustrates that while glucocorticoids may be a contributor to the magnitude of difference between cell models, it is not the sole source of the variances. HepG2 cells and HLCs were maintain in cell culture medium containing glucose in supra-physiological levels which consequently enables cells to generate energy through glycolysis as opposed to oxidative phosphorylation. The use of *in vitro* protocols which do not maintain hepatocytes *ex vivo* in a physiologically applicable environment could underpin many of the number of differences observed across the proteome.

Irrespective of the limitations of the cell culture microenvironment, clustering of HLCs and PHHs in Component 1 is suggests that despite HLCs being cultured as monolayers that the proteomes of PHHs and HLCs most closely related. Successful differentiation of hiPSCs to HLCs is a complex interplay of cell proliferation and maturation. The duration of differentiation and resultant degree of maturity influences the degree to which HLCs mimic PHHs. Therefore, differentiation beyond a critical threshold could underestimate the proteomic correlation between hiPSC-HLCs and PHHs. Other recent work by Asai *et al.* found that HLCs with spatial proximity to human umbilical vein endothelial cells or mesenchymal stem cells which provide paracrine signals could more closely aligned the HLC proteome with that of PHHs (Asai A *et al.*, 2017). This suggests that using this differentiation protocol with additional paracrine signalling could enhance the HLCs protein complement to be even more representative of PHHs. These proteomic data described may contain noteworthy insights of essential contributors to the HLC proteome.

Major differences between PHHs and HepG2 cells include morphology, the transformed and discontinuous phenotype of cancer cells as well as maintenance of cells in culture (Wilkening S *et al.*, 2003). In addition, HepG2 cells vary in their overall metabolic, glycolytic and anaerobic activity functions with the low number of mRNA copies and protein expression of essential phase I enzymes (Duret C *et al.*, 2007; Wilkening S *et al.*, 2003). This study further reiterates the need to limit the use

of short-term HepG2 cell monolayer cultures. Comparing the proteomes of PHHs to HepG2 3D spheroids identified less abundance variances than in HepG2 monolayer counterparts. Luckert *et al.* (2017) observed that metabolic competence of HepG2 cells grown as monolayers for 21 days had comparable biochemical characteristics to HepG2 cells grown in various 3D culture formats (Luckert C *et al.*, 2017). This suggests differences in any metabolic proteins seen here could be as a result of the longer culturing of HepG2 cells as 3D spheroids of ten days as opposed to 3 days in monolayer culture. Despite the extended culture duration, hierarchical clustering and PCA were unable to distinguish HepG2 monolayer and 3D spheroid cultures. Here, under the conditions investigated, HepG2 cells as 3D spheroids would not confer major alteration in biochemical characteristics. Instead, culturing HepG2 cells without adherence to artificial substrates which augmented cell morphology was considered as a main contributor to the reduced number of significantly different proteins compared to PHHs.

Conclusions

Here, the use of quantitative isobaric-labelled proteomics and careful preparation steps resulted in over 6000 proteins being positively identified per replicate with high confidence to compare PHHs, HLCs and HepG2 cells. This quantitative data provides biological insight into the feasibility of using HLCs, HepG2 monolayers and HepG2 3D spheroids as hepatotoxicity models. Since cellular homeostasis, cellular growth and hepatic maturity are dynamic processes the cellular proteome data described in this study represents a "*snapshot*" of the proteome. These data supports the concept that there is, no single hepatic model that can accurately reflect the diverse array of outcomes required to mimic the *in vivo* liver functions as of yet. None of the models are considered a feasible substitute to PHHs, however, these data reveals how differentiated HLCs and HepG2 cells under different culturing techniques differ in relative abundance of proteins compared to PHHs. The proteome of the HLCs, under the conditions investigated, better correlated to PHHs than the HepG2 monolayers or 3D spheroid counterparts. It is proposed that these data could provide insights into improving hepatocyte models and aid in enhancing the mimicry of the *in vivo* hepatic phenotype.

Author's contribution

TH, ADC and KSL designed and planned the experiments. TH and CPS performed the cell culture and differentiation procedures. TH performed protein sample preparation and data analysis. All authors contributed to the data interpretation and to the writing of the manuscript. None of the authors declare any competing interests.

Funding information

This research was supported in part by the National Research Foundation of South Africa for the grant (Grant No. 87880.) TH was supported by a UK Commonwealth Split-site PhD Scholarship (ZACS-2014-653) and a Commonwealth, European and International Cambridge Trust Scholarship (USN: 302989247; App No: 10326363). CPS was funded by Children Liver Disease foundation PhD studentship and LV by the ERC starting Grant Relieve IMD. Any opinion, finding, conclusion or recommendation expressed in this material is that of the author(s) and not the funding agencies mentioned.

Acknowledgements

We would like to thank Dr Mike Deery at the Cambridge Centre for Proteomics for assistance with the mass spectrometry and Dr Stoyan Stoychev at the South African Council for Scientific and Industrial Research who provided the infrastructure required for the bioinformatics data analysis.

References

Asai A., Aihara E., Watson C., Mourya R., Mizuochi T., Shivakumar P., Phelan K., Mayhew C., Helmrath M. and Takebe T. (2017). Paracrine signals regulate human liver organoid maturation from induced pluripotent stem cells. *Development* **144**(6), 1056-1064.

Ballet F. (1997). Hepatotoxicity in drug development: Detection, significance and solutions. *J. Hepatol.* **26**, 26-36.

Baxter M., Withey S., Harrison S., Segeritz C. P., Zhang F., Atkinson-Dell R., Rowe C., Gerrard D. T., Sison-Young R. and Jenkins R. (2015). Phenotypic and functional analyses show stem cell-derived hepatocyte-like cells better mimic fetal rather than adult hepatocytes. *J. Hepatol.* **62**(3), 581-589.

Bell C. C., Hendriks D. F., Moro S. M., Ellis E., Walsh J., Renblom A., Puigvert L. F., Dankers A. C., Jacobs F. and Snoeys J. (2016). Characterization of primary human hepatocyte spheroids as a model system for drug-induced liver injury, liver function and disease. *Sci. Rep.* **6**, 25187.

Bhadriraju K. and Chen C. S. (2002). Engineering cellular microenvironments to improve cell-based drug testing. *Drug Discovery Today* **7**(11), 612-620.

Cai J., DeLaForest A., Fisher J., Urick A., Wagner T., Twaroski K., Cayo M., Nagaoka M. and Duncan S. A. (2012). Protocol for directed differentiation of human pluripotent stem cells toward a hepatocyte fate. *StemBook*.

DiMasi J. A., Hansen R. W. and Grabowski H. G. (2003). The price of innovation: New estimates of drug development costs. *J. Health Econ.* **22**(2), 151-185.

Duret C., Gerbal-Chaloin S., Ramos J., Fabre J. M., Jacquet E., Navarro F., Blanc P., Sa-Cunha A., Maurel P. and Daujat-Chavanieu M. (2007). Isolation, characterization, and differentiation to hepatocyte-like cells of nonparenchymal epithelial cells from adult human liver. *Stem Cells* **25**(7), 1779-1790.

Fey S. J. and Wrzesinski K. (2012). Determination of drug toxicity using 3d spheroids constructed from an immortal human hepatocyte cell line. *Toxicol. Sci.* **127**(2), 403-411.

Hannan N. R., Segeritz C. P., Touboul T. and Vallier L. (2013). Production of hepatocyte-like cells from human pluripotent stem cells. *Nat. Protoc.* **8**(2), 430-437.

Kessner D., Chambers M., Burke R., Agus D. and Mallick P. (2008). Proteowizard: Open source software for rapid proteomics tools development. *Bioinformatics* **24**(21), 2534-2536.

Knasmüller S., Mersch-Sundermann V., Kevekordes S., Darroudi F., Huber W., Hoelzl C., Bichler J. and Majer B. (2004). Use of human-derived liver cell lines for the detection of environmental and dietary genotoxicants: Current state of knowledge. *Toxicology* **198**(1), 315-328.

LeCluyse E. L., Witek R. P., Andersen M. E. and Powers M. J. (2012). Organotypic liver culture models: Meeting current challenges in toxicity testing. *Crit. Rev. Toxicol.* **42**(6), 501-548.

Lemaigre F. (2010). Markers and signaling factors for stem cell differentiation to hepatocytes: Lessons from developmental studies. *Hepatocytes: Methods and Protocols* **640**, 157-166.

Luckert C., Schulz C., Lehmann N., Thomas M., Hofmann U., Hammad S., Hengstler J. G., Braeuning A., Lampen A. and Hessel S. (2017). Comparative analysis of 3d culture methods on human hepg2 cells. *Arch. Toxicol.* **91**(1), 393-406.

Mills J. B., Rose K. A., Sadagopan N., Sahi J. and de Morais S. M. (2004). Induction of drug metabolism enzymes and mdr1 using a novel human hepatocyte cell line. *J. Pharmacol. Exp. Ther.* **309**(1), 303-309.

Mingard C., Paech F., Bouitbir J. and Krähenbühl S. (2018). Mechanisms of toxicity associated with six tyrosine kinase inhibitors in human hepatocyte cell lines. *J. Appl. Toxicol.* **38**(3), 418-431.

Paech F., Mingard C., Grünig D., Abegg V. F., Bouitbir J. and Krähenbühl S. (2018). Mechanisms of mitochondrial toxicity of the kinase inhibitors ponatinib, regorafenib and sorafenib in human hepatic hepg2 cells. *Toxicology*.

Peters T. S. (2005). Do preclinical testing strategies help predict human hepatotoxic potentials? *Toxicol. Pathol.* **33**(1), 146-154.

Psarra A.-M. G. and Sekeris C. E. (2011). Glucocorticoids induce mitochondrial gene transcription in hepg2 cells: Role of the mitochondrial glucocorticoid receptor. *Biochimica et Biophysica Acta (BBA)-Molecular Cell Research* **1813**(10), 1814-1821.

Ramirez T., Strigun A., Verlohner A., Huener H.-A., Peter E., Herold M., Bordag N., Mellert W., Walk T. and Spitzer M. (2018). Prediction of liver toxicity and mode of action using metabolomics in vitro in hepg2 cells. *Arch. Toxicol.* **92**(2), 893-906.

Rashid S. T., Corbineau S., Hannan N., Marciniak S. J., Miranda E., Alexander G., Huang-Doran I., Griffin J., Ahrlund-Richter L. and Skepper J. (2010). Modeling inherited metabolic disorders of the liver using human induced pluripotent stem cells. *The Journal of Clinical Investigation* **120**(9), 3127-3136.

Redfern W. S., Wakefield I. D., Prior H., Pollard C. E., Hammond T. G. and Valentin J. P. (2002). Safety pharmacology – a progressive approach. *Fundam. Clin. Pharmacol.* **16**(3), 161-173.

Schwartz R., Fleming H., Khetani S. and Bhatia S. (2014). Pluripotent stem cell-derived hepatocyte-like cells. *Biotechnology Advances* **32**(2), 504-513.

Shah U.-K., de Oliveira Mallia J., Singh N., Chapman K. E., Doak S. H. and Jenkins G. J. (2018). A three-dimensional in vitro hepg2 cells liver spheroid model for genotoxicity studies. *Mutation Research/Genetic Toxicology and Environmental Mutagenesis* **825**, 51-58.

Si-Tayeb K., Noto F. K., Nagaoka M., Li J., Battle M. A., Duris C., North P. E., Dalton S. and Duncan S. A. (2010). Highly efficient generation of human hepatocyte–like cells from induced pluripotent stem cells. *Hepatology* **51**(1), 297-305.

Sison-Young R. L., Mitsa D., Jenkins R. E., Mottram D., Alexandre E., Richert L., Aerts H., Weaver R. J., Jones R. P. and Johann E. (2015). Comparative proteomic characterization of 4 human liver-derived single cell culture models reveals significant variation in the capacity for drug disposition, bioactivation, and detoxication. *Toxicol. Sci.* **147**(2), 412-424.

TheUniProtConsortium (2014). Uniprot: A hub for protein information. Nucleic Acids Res. **43:** 204-212.

Uhlén M., Fagerberg L., Hallström B. M., Lindskog C., Oksvold P., Mardinoglu A., Sivertsson Å., Kampf C., Sjöstedt E. and Asplund A. (2015). Tissue-based map of the human proteome. *Science* **347**(6220), 394-404.

Vaudel M., Barsnes H., Berven F. S., Sickmann A. and Martens L. (2011). Searchgui: An open-source graphical user interface for simultaneous omssa and x! Tandem searches. *Proteomics* **11**(5), 996-999.

Vaudel M., Burkhart J. M., Zahedi R. P., Oveland E., Berven F. S., Sickmann A., Martens L. and Barsnes H. (2015). Peptideshaker enables reanalysis of ms-derived proteomics data sets. *Nat. Biotechnol.* **33**(1), 22-24.

Vorrink S. U., Ullah S., Schmidt S., Nandania J., Velagapudi V., Beck O., Ingelman-Sundberg M. and Lauschke V. M. (2017). Endogenous and xenobiotic metabolic stability of primary human hepatocytes in long-term 3d spheroid cultures revealed by a combination of targeted and untargeted metabolomics. *The FASEB Journal* **31**(6), 2696-2708.

Wilkening S., Stahl F. and Bader A. (2003). Comparison of primary human hepatocytes and hepatoma cell line hepg2 with regard to their biotransformation properties. *Drug Metabolism and Disposition* **31**(8), 1035-1042.

Xu J. J., Diaz D. and O'Brien P. J. (2004). Applications of cytotoxicity assays and pre-lethal mechanistic assays for assessment of human hepatotoxicity potential. *Chem. Biol. Interact.* **150**(1), 115-128.

Yusa K., Rashid S. T., Strick-Marchand H., Varela I., Liu P., Paschon D. E., Miranda E., Ordóñez A., Hannan N. R. and Rouhani F. J. (2011). Targeted gene correction of alpha-1-antitrypsin deficiency in induced pluripotent stem cells. *Nature* **478**, 391-394.

Figure legends

Figure 1: Phase contrast images (EVOS FL Cell Imaging System) showing differentiation of human induced pluripotent stem cells (hiPSCs) into hepatocyte-like cells (HLCs). A) hiPSCs organised in tightly packed colonies, B) Definitive endoderm specification with cellular migration from the colony, C) Foregut or anterior definitive endoderm cells, D) Hepatic endoderm, E-F) Hepatocyte-like cell maturation. CDM-PVA: chemically defined medium with polyvinyl alcohol, FGF: fibroblast growth factor, BMP: bone morphogenic protein, HGF: hepatocyte growth factor. Scale bar: 400 µm. (Reprinted/redrawn from open access journal with permission, (Hannan NR et al., 2013)).

Figure 2: Phase contrast images (EVOS FL Cell Imaging System) of A) Hepatocyte-like cell monolayers differentiation at day 35, B) HepG2 cell monolayers on day 1 after seeding which were harvested once at confluence, C) HepG2 cell 3D spheroids at day 10 of culture (scale bar: 200 µm), D) Coomassie stained 4-15% Mini-PROTEAN TGX gel of hepatocyte lysates. Lane 1 and 10: St: Precision Plus Protein Dual Colour standard (2-250kDa), Lanes 2 and 4: HepG2 cell 3D spheroids collected on day 10, Lane 3: HepG2 cell spheroids collected at day 14, Lane 5 to 7: HepG2 cell monolayers at various passages, Lane 8 and 9: primary human hepatocytes.

Figure 3: A) Hierarchical clustering of proteomic data for individual samples, B) Protein profile trends produced from hierarchical clustering (10 row clusters) with the corresponding number of grouped proteins. Clusters 9 and 10 (not included) contained a single protein only.

Figure 4: Principal components analysis scatter plots of A) Component 1 versus Component 2, B) Component 1 versus Component 3. PHHs (n=4, triangle), HLCs (n=6, square), HepG2 monolayers (n=4, circle), HepG2 spheroids (n=3, diamond).

Figure 5: Volcano plots comparing PHHs to HLCs, PHHs to HepG2 monolayers and PHHs to HepG2 3D spheroids. Proteins plotted above and to the left or right of the significance discriminant line are differentially increased or decreased abundance relative to PHHs respectively using an FDR of 0.01. Proteins which displayed significant differences between PHH and each model are provided (Supplementary data 2: volcano plots for PHHvHLCs, PHHvHepG2 and PHHvHepG2(3D)).

Tables:

Table 1: Comparison of proteins with the same or different abundance between models

	HLCs	HepG2 monolayers	HepG2 3D spheroids
Proteins with higher abundance in PHHs compared to each model	1020	1327	682
Proteins with significantly lower abundance in PHHs compared to each model	961	956	180
	HLCs versus HepG2 monolayers	**HLCs versus HepG2 3D spheroids**	**HepG2 monolayers versus 3D spheroids**
Comparison of the overlap of proteins with higher abundance in PHHs	751	500	653
Comparison of the overlap of proteins with lower abundance in PHHs	282	66	142
Variable differences	62	11	0

Footnote Table 1: Proteins with higher abundance in PHHs (right of volcano plot) or proteins with lower abundance in PHHs (left of volcano plot) for HLCs, HepG2 monolayers or HepG2 3D spheroids were first extracted. These proteins were then compared between HLCs, HepG2 monolayers and HepG2 3D spheroids to determine if the overlap of proteins meeting the same cut-offs on the volcano plot were similar. For instance 1020 proteins were higher in PHH compared to HLCs and this was compared to the 1327 proteins for HepG2 monolayers and 751 of these were the same protein.

Table 2: Statistical significance of proteins involved in metabolism compared using multiple sample testing (ANOVA) or two-tailed t-test

		Multiple sample testing	Significance following two-tailed t-tests		
Protein description	**Main accession**	**ANOVA significance**	**PHHs versus HLCs**	**PHHs versus HepG2 monolayer**	**PHHs versus HepG2 3D spheroids**
Alcohol dehydrogenase [NADP(+)]	P14550	+	-	+	+
Alcohol dehydrogenase 1A	P07327	+	+	+	+
Alcohol dehydrogenase 1B	P00325	+	+	+	+
Alcohol dehydrogenase 1C	P00326	+	+	+	+
Alcohol dehydrogenase 4	P08319	+	+	+	+
Alcohol dehydrogenase 6	P28332	+	+	+	-
Alcohol dehydrogenase class-3	P11766	+	-	+	-
Aldehyde dehydrogenase family 16 member A1	Q8IZ83	+	+	+	-
Aldehyde dehydrogenase family 8 member	Q9H2A2	+	+	+	+
Aldehyde dehydrogenase X, mitochondrial	P30837	+	+	+	+
Aldehyde dehydrogenase, mitochondrial	P05091	+	+	+	+
Aldehyde oxidase	Q06278	+	+	+	+
Aldo-keto reductase family 1 member B10	O60218	+	-	-	+
Aldo-keto reductase family 1 member C1	Q04828	+	+	-	-
Aldo-keto reductase family 1 member C2	P52895	+	+	+	-
Aldo-keto reductase family 1 member C3	P42330	+	+	+	-
Aldo-keto reductase family 1 member C4	P17516	+	+	+	-
Cytochrome b5	P00167	+	+	+	+
Cytochrome P450 1A1	P04798	+	+	+	+
Cytochrome P450 1A2	P05177	+	+	+	+
Cytochrome P450 20A1	Q6UW02	+	+	+	+
Cytochrome P450 2A6	P11509	+	+	+	+
Cytochrome P450 2B6	P20813	+	+	+	-
Cytochrome P450 2C19	P33261	+	+	+	+
Cytochrome P450 2C8	P10632	+	+	+	-
Cytochrome P450 2C9	P11712	+	+	+	+
Cytochrome P450 2D6	P10635	+	+	+	+
Cytochrome P450 2E1	P05181	+	+	+	+
Cytochrome P450 2J2	P51589	+	+	+	+
Cytochrome P450 2S1	Q96SQ9	+	+	+	-

Cytochrome P450 2W1	Q8TAV3	+	-	-	-
Cytochrome P450 3A4	P08684	+	+	+	+
Cytochrome P450 3A5	P20815	+	+	+	+
Cytochrome P450 4A11	Q02928	+	+	+	+
Cytochrome P450 4F12	Q9HCS2	+	+	+	-
Cytochrome P450 4V2	Q6ZWL3	+	+	+	+
Dimethylaniline monooxygenase [N-oxide-forming] 3	P31513	+	+	+	+
Dimethylaniline monooxygenase [N-oxide-forming] 4	P31512	+	+	+	+
Dimethylaniline monooxygenase [N-oxide-forming] 5	P49326	+	+	+	+
Gamma-glutamyltranspeptidase 1	P19440	+	+	+	-
Glutathione reductase, mitochondrial	P00390	+	-	+	-
Glutathione S-transferase A2	P09210	+	-	+	+
Glutathione S-transferase C-terminal domain-containing protein	Q8NEC7	+	-	+	-
Glutathione S-transferase kappa 1	Q9Y2Q3	+	-	+	+
Glutathione S-transferase Mu 1	P09488	+	+	+	+
Glutathione S-transferase Mu 2	P28161	-	-	-	-
Glutathione S-transferase Mu 3	P21266	+	+	-	-
Glutathione S-transferase omega-1	P78417	+	-	+	-
Glutathione S-transferase P	P09211	+	+	-	-
Glutathione S-transferase theta-1	P30711	+	+	+	-
Glutathione S-transferase theta-2	P0CG29	+	+	+	+
Glutathione synthetase	P48637	-	-	-	-
Multidrug resistance protein 1	P08183	+	+	-	-
Multidrug resistance-associated protein 1	P33527	+	+	+	-
Multidrug resistance-associated protein 6	O95255	+	+	+	+
NADPH--cytochrome P450 reductase	P16435	+	-	+	+
UDP-glucuronosyltransferase 1-1	P22309	+	+	+	+
UDP-glucuronosyltransferase 1-4	P22310	+	+	+	+
UDP-glucuronosyltransferase 1-6	P19224	+	+	+	+
UDP-glucuronosyltransferase 2A3	Q6UWM9	+	+	+	-
UDP-glucuronosyltransferase 2B10	P36537	+	+	+	+
UDP-glucuronosyltransferase 2B15	P54855	+	+	+	+
UDP-glucuronosyltransferase 2B17	O75795	+	+	+	+
UDP-glucuronosyltransferase 2B4	P06133	+	+	+	-
UDP-glucuronosyltransferase 2B7	P16662	+	+	+	+

Footnote Table 2: The average relative abundance and standard deviarion across replicates provided in Supplementary data 2: Metabolic proteins.

Figures:

Figure 1:

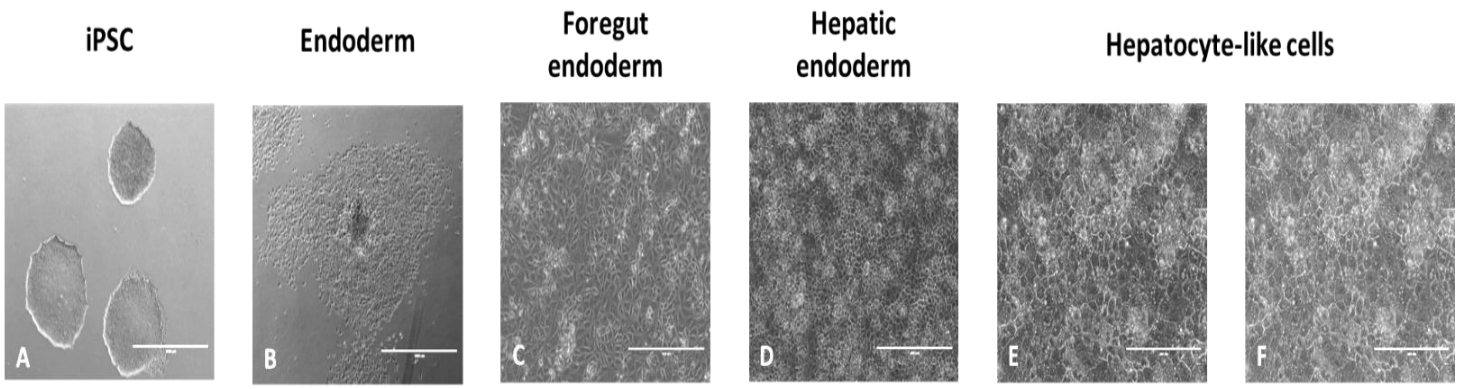

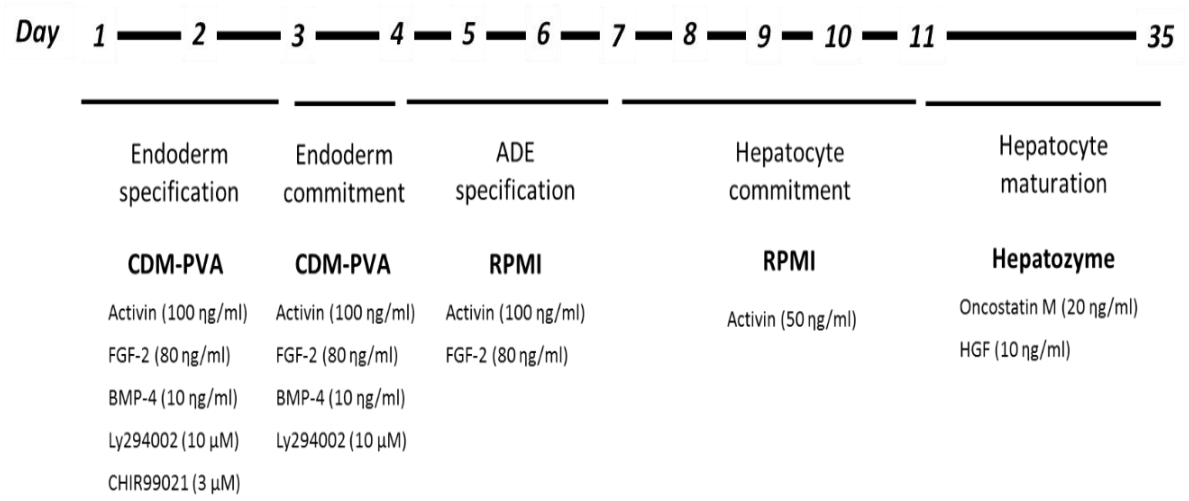

Figure 2:

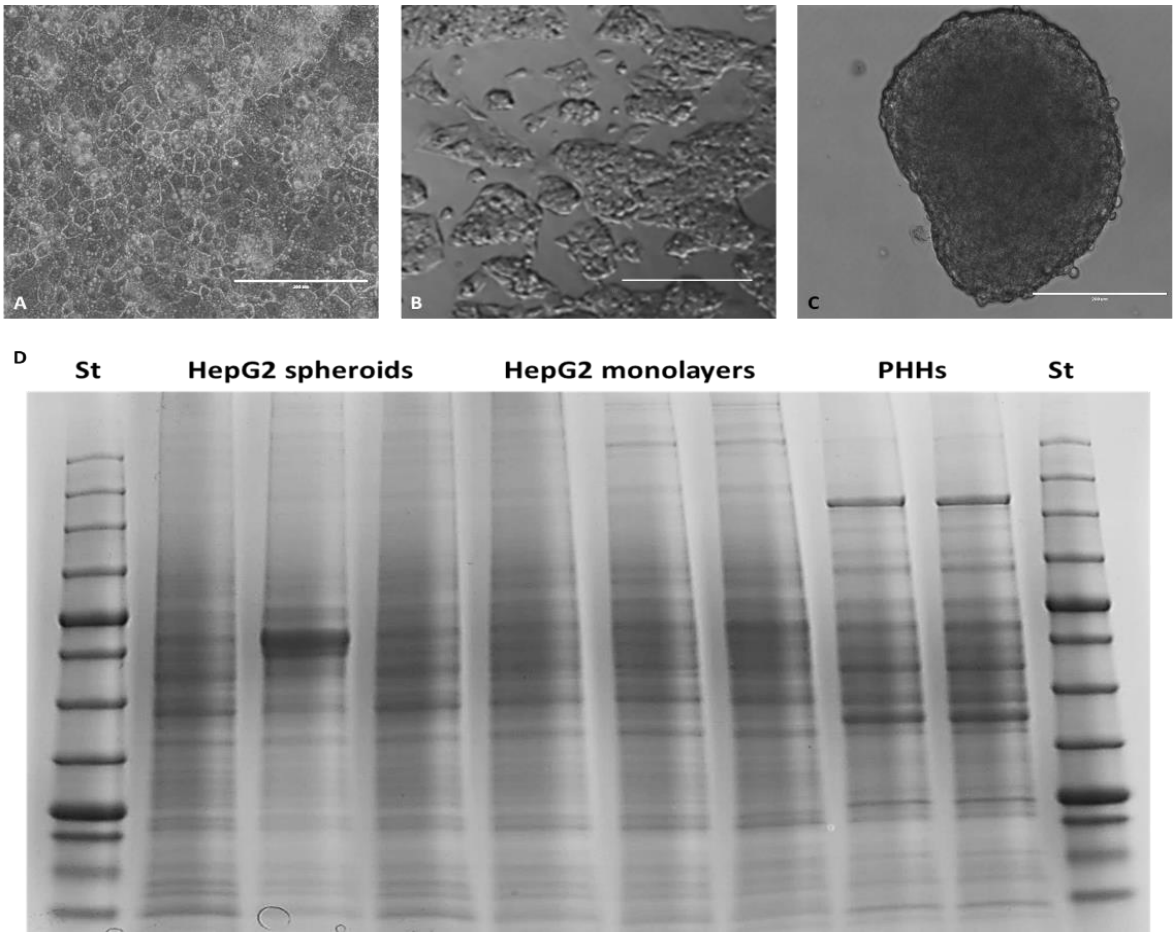

Figure 3:

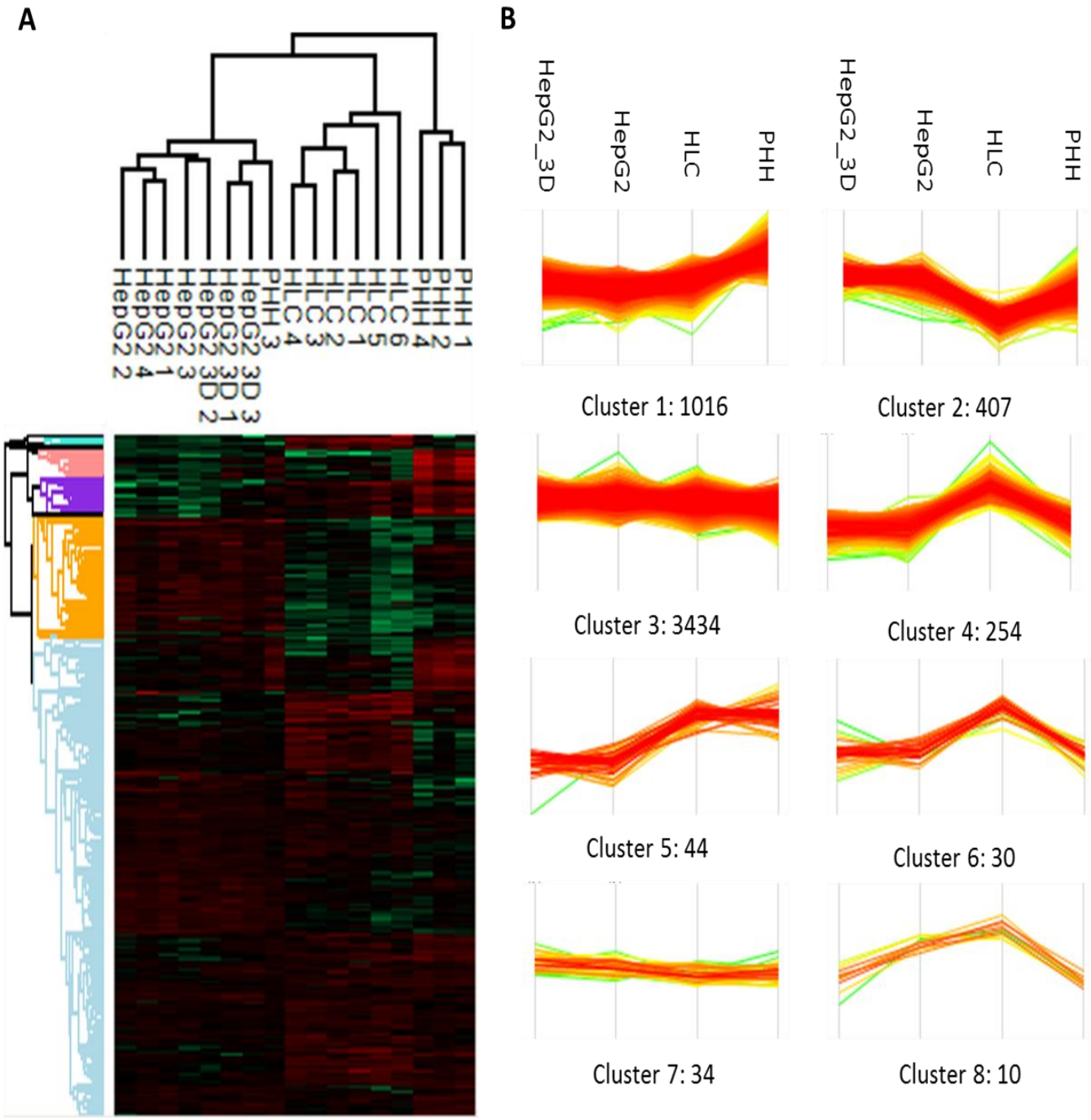
A
PHH 1
PHH 2
PHH 4
HLC 6
HLC 5
HLC 1
HLC 2
HLC 3
HLC 4
PHH 3
HepG2 3D 3
HepG2 3D 1
HepG2 3D 2
HepG2 2 1
HepG2 2 4
HepG2 2 3
HepG2 2 2
B
HepG2_3D
HepG2
HLC
PHH
Cluster 1: 1016
Cluster 2: 407
Cluster 3: 3434
Cluster 4: 254
Cluster 5: 44
Cluster 6: 30
Cluster 7: 34
Cluster 8: 10

Figure 4:

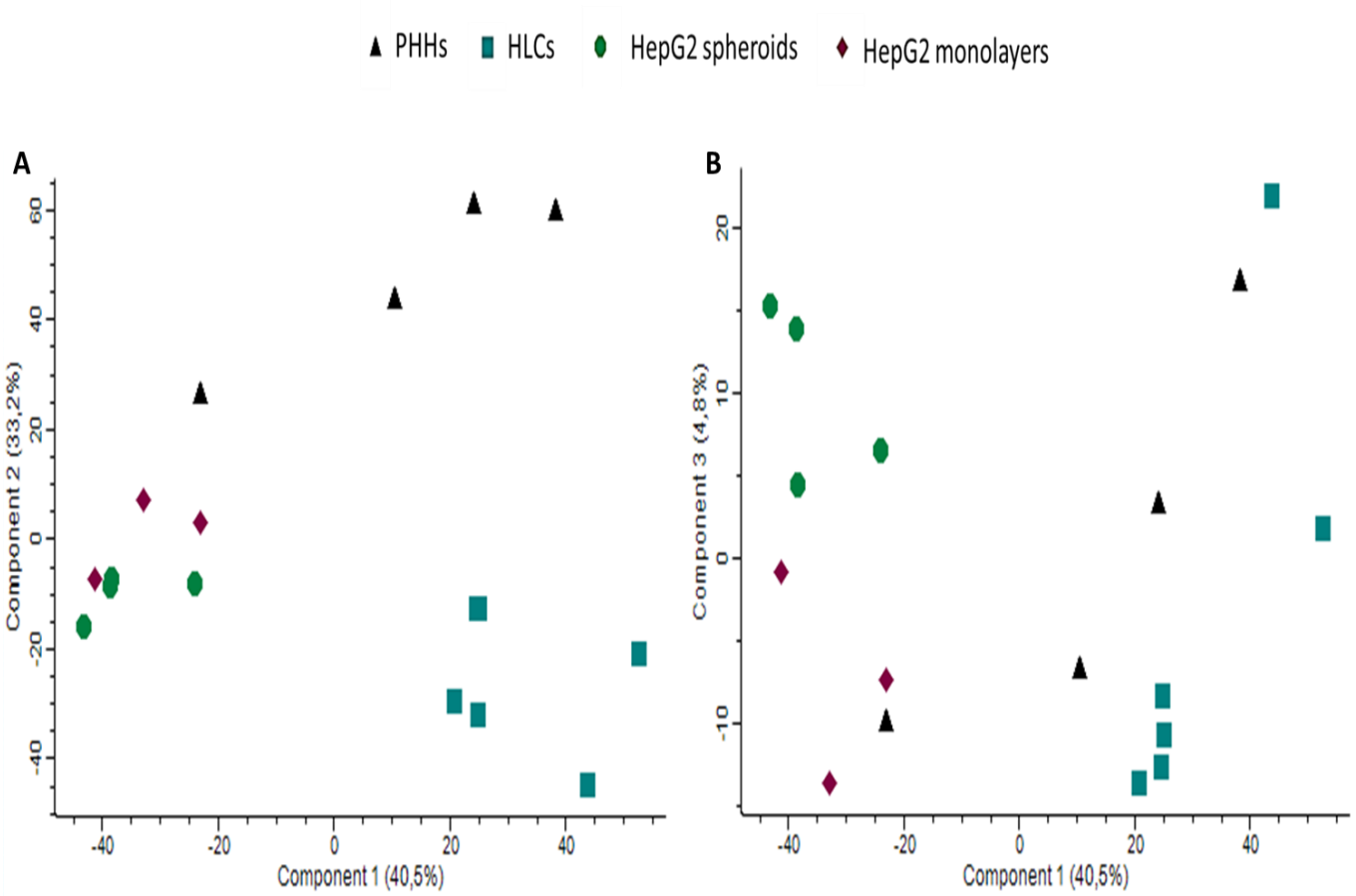

Figure 5: